Indonesian Journal of Aerospace Vol. 21 No. 1 Juni 2023 : pp 1 – 12 (Ruseno)
DOI: 10.59981/ijoa.2023.302
https://ejournal.brin.go.id/ijoa/

Stability Analysis of 3D UAV Gimbal using Flexible Body

Neno Ruseno

Aviation Engineering Department, International University Liaison Indonesia, Indonesia
e-mail: neno.ruseno@iuli.ac.id

Received:28-02-2023. Accepted: 04-04-2023. Published: 30-06-2023

Abstract

Unmanned aerial vehicle (UAV) application in visual object tracking requires a gimbal to stabilize the camera in following the object's movement. External disturbance and gimbal stability are the issues in this application. This study aims to analyze disturbance effects and study the stress and modal analysis on UAV gimbal using flexible body concepts. The three-dimensional (3D) gimbal is modeled using the RecurDyn software consisting of 3 arms and a camera. Each of the arms is connected using a revolute joint and a rotational force to represent a motor. The considered disturbances are step, pulse, ramp, and sine wave input. The PID controller is used to stabilize the gimbal arm from the gravity of the camera and external disturbance. The result shows that the PID controller is robust to step, pulse, and ramp disturbance, but not to the sin wave disturbance. In addition, the second arm of the gimbal is the most stressed component and is prone to vibration.

Keywords: *3D UAV gimbal; RecurDyn; PID controller; stability analysis; flexible body.*

1. Introduction

One of the reasons that make unmanned aerial vehicles (UAVs) popular is their capability to bring a camera and take pictures from a point that humans never see it. Visual object tracking is one of the UAV applications based on that capability. However, there are many disturbances to the UAV flight that could reduce the image quality. Gimbal is one of the solutions to that issue which can provide a stable platform that is undisturbed from external disturbances.

Based on the latest research development, UAVs equipped with a camera mounted on a gimbal can be used for visual object tracking (Krakow et al., 2018; Sun et al., 2008), (Park et al., 2019). The first research formulated the problem as a partially observable Markov decision process (POMDP) and applied a Q-value approximation technique named nominal belief-state optimization (NBO). It combined with a heuristic expected cost-to-go (HECTG) to improve the target-tracking performance at an acceptable computational speed (Krakow et al., 2018). With a less trajectory dimension compared to the first research, the second research created two-dimensional (2D) trajectories of the gimbal mounted on a UAV based on the UAV location and provided the guidance law of the path following system (Sun et al., 2008). If the first two research conducted moving object tracking, the third research explored static object tracking. It developed an auto-tracking camera gimbal that automatically tracks and photographs power facilities using a Deep Learning algorithm (Park et al., 2019).

Besides far-distance object tracking, a gimbal also can be used for near-object tracking such as the human body (Sayed et al., 2022; Zhao et al., 2022). Research on machine vision using the OpenCV algorithm employed a camera mounted on a gimbal to identify and track a human presenter. The system was able to control the camera pan-tilt function and automatically track the presenter's movements (Zhao et al., 2022). Similarly, another research developed the LookOut system which was built based on a lightweight commodity camera gimbal mechanism with major modifications to the controller. The system could react to speech commands, gestures, and a premade script for filming camera purposes (Sayed et al., 2022).

The second application type of gimbal in UAV is an attitude stabilizer to provide a stable camera platform (Tiimus & Tamre, 2010), (Lin & Yang, 2014), (Basu et al., 2019). Research developed a prototype gimbal mechanism with 3-axis gearhead DC motors that implemented an incremental encoder feedback and Attitude and Heading reference system (AHRS) unit for angular movement feedback (Tiimus & Tamre, 2010). Another research implemented GPS and UAV attitude estimation from the gimbal about the tracking target to develop a reliable autopilot for photography purposes (Lin & Yang, 2014). Similarly, a control system in Arduino-based UAV was developed and simulated for the stability of the camera position by MATLAB Simulink. The control system was implemented in a three axes gimbal for holding and controlling the orientation of the camera (Basu et al., 2019).

The last gimbal application is more related to UAV flight missions (Tang et al., 2019), (Geng et al., 2014), (Springer & Kyas, 2022). Research on the problem of mission planning with UAVs for urban surveillance was conducted. A gimbal combined with evolutionary algorithms such as PSO and GA had been developed for optimization to deal with situations with/ without the enemy presence (Tang et al., 2019).

This study aims to analyze disturbance effects on UAV gimbal stability and to study stress and modal analysis using flexible body concepts. The result can be used in designing a gimbal for UAV applications. This report consists of the background theory in chapter 2 and the methodology in chapter 3. The result and analysis are in chapter 4. The last chapter is the conclusion and recommendation.

2. Background Theory

In this section, the basic knowledge of gimbal modeling, PID controller, and flexible body is explained.

2.1. Gimbal Modelling

The 3D gimbal consists of three axes represented by three revolute joints connecting its arms. The angle of its axis is named yaw, roll, and pitch ($\theta_1\theta_1$, $\theta_2\theta_2$, $\theta_3\theta_3$) as shown in Figure 2-1(Rajesh & Kavitha, 2015).

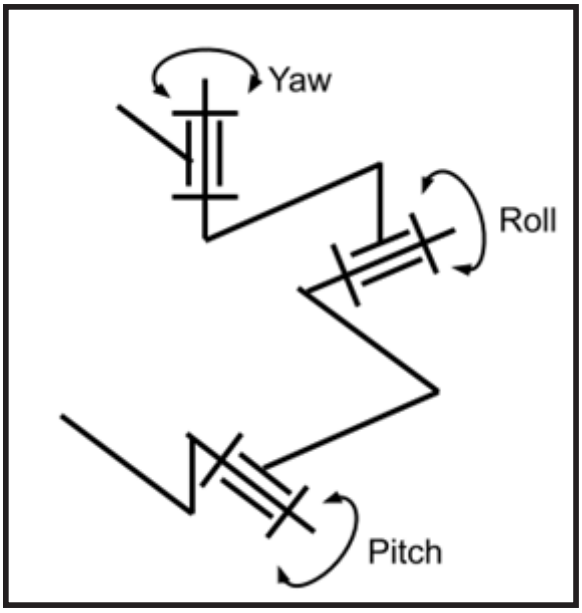

Figure 2-1: 3D gimbal kinematic with 3 joints and angles

The gimbal kinematics equations can be derived from the transformation of body coordinates from body 0 to body 3 (Rajesh & Kavitha, 2015). The rotation matrix of the yaw axis from body frame 0 to body frame 1 is shown in Eq. (2-1).

$$ {}^{0}\boldsymbol{R_1} = \begin{bmatrix} cos\ \theta_1 & -sin\ \theta_1 & 0 \\ sin\ \theta_1 & cos\ \theta_1 & 0 \\ 0 & 0 & 1 \end{bmatrix} \quad (2\text{-}1) $$

The rotation matrix of the roll axis from body frame 1 to body frame 2 is shown in Eq. (2-2).

$$^{1}\boldsymbol{R}_{\boldsymbol{2}} = \begin{bmatrix} 1 & 0 & 0 \\ 0 & cos\,\theta_2 & -sin\,\theta_2 \\ 0 & sin\,\theta_2 & cos\,\theta_2 \end{bmatrix} \quad (2\text{-}2)$$

The rotation matrix of the pitch axis from body frame 3 to body frame 3 is shown in Eq. (2-3).

$$^{2}\boldsymbol{R}_{\boldsymbol{3}} = \begin{bmatrix} cos\,\theta_3 & 0 & sin\,\theta_3 \\ 0 & 1 & 0 \\ -sin\,\theta_3 & 0 & cos\,\theta_3 \end{bmatrix} \quad (2\text{-}3)$$

The total rotation matrix between body frame 0 to body frame 3 is shown in Eq. (2-4).

$$^{0}\boldsymbol{R}_{\boldsymbol{3}} = \begin{bmatrix} C_1C_3 - S_1S_2S_3 & -C_2S_1 & C_1C_3 + C_3S_1S_2 \\ C_3S_1 + C_1S_2S_3 & C_1C_2 & S_1S_3 - C_1C_3S_2 \\ -C_2S_3 & S_2 & C_2C_3 \end{bmatrix} \quad (2\text{-}4)$$

Where: $C_i = cos\,\theta_i$ and $S_i = sin\,\theta_i$

The inertia measurement unit (IMU) sensor is mounted on the camera frame (body frame 3) to measure angles of yaw, roll, and pitch (α_1, α_2, α_3). The desired angle of the camera is presented by ($\alpha_{1desired}$, $\alpha_{2desired}$, $\alpha_{3desired}$). The error of yaw, roll, and pitch angle is calculated in Eq. (2-5)

$$\varepsilon_i = \alpha_{i\,desired} - \alpha_i \quad (2\text{-}5)$$

Where i = 1, 2, and 3

The rotation matrix of the camera's error reference frame is shown in Eq. (2-6).

$$^{0}\boldsymbol{R}_{\boldsymbol{\varepsilon}} = \begin{bmatrix} C\varepsilon_1C\varepsilon_3 - S\varepsilon_1S\varepsilon_2S\varepsilon_3 & -C\varepsilon_2S\varepsilon_1 & C\varepsilon_1C\varepsilon_3 + C\varepsilon_3S\varepsilon_1S\varepsilon_2 \\ C\varepsilon_3S\varepsilon_1 + C\varepsilon_1S\varepsilon_2S\varepsilon_3 & C\varepsilon_1C\varepsilon_2 & S\varepsilon_1S\varepsilon_3 - C\varepsilon_1C\varepsilon_3S\varepsilon_2 \\ -C\varepsilon_2S\varepsilon_3 & S\varepsilon_2 & C\varepsilon_2C\varepsilon_3 \end{bmatrix} \quad (2\text{-}6)$$

Where: $C\varepsilon_i = cos\,\varepsilon_i$ and $S\varepsilon_i = sin\,\varepsilon_i$

From the inverse kinematics of the gimbal, the total rotation matrix from body frame 0 to camera error reference frame is shown in Eq. (2-7).

$$^{0}\boldsymbol{R}_{\boldsymbol{\varepsilon}}\,(\theta, \varepsilon) = {}^{0}\boldsymbol{R}_{\boldsymbol{3}}\,(\theta)\;{}^{3}\boldsymbol{R}_{\boldsymbol{\varepsilon}}\,(\varepsilon) \quad (2\text{-}7)$$

Since θ_1, θ_2, and θ_3 are the current joint angles, the new joint gimbal angles are calculated in Eq. (2-8).

$$^{0}\boldsymbol{R}_{\boldsymbol{\varepsilon}}\,(\theta_{new}) = {}^{0}\boldsymbol{R}_{\boldsymbol{\varepsilon}}\,(\boldsymbol{\theta}, \varepsilon) \quad (2\text{-}8)$$

2.2. PID Controller

PID controller is widely used to control many industry applications employing feedback loop control mechanism. Its parameters consist of proportional, integral, and differential gain (Rajesh & Ananda, 2015). The PID controller transfer function is shown in Eq. (2-9)

$$G_{PID} = K_P + \frac{K_I}{s} + K_D s \quad (2\text{-}9)$$

where:

K_P = proportional gain

K_I = integral gain

K_P = differential gain

s = Laplace operator

The overall controller is very sensitive to the magnitude of each gain. The proportional gain generates a result that is proportional to the current error magnitude. However, the integral gain is proportional to both the magnitude of the error and the duration of the error. In addition, the derivative gain determines the slope of the error over time (Wikipedia, 2023).

2.3. Flexible Body

In general, a gimbal can be considered a combination of a rigid body and a flexible body. The transfer function of a gimbal having both rigid and flexible body characteristics is shown in Eq. (2-10) (Bansal & Dewan, 2014):

$$\frac{(\theta+\delta\theta)(s)}{\theta(s)} = \left(\frac{1}{sI_1+B}\right)\left(\frac{s^2+2\xi\omega_{s1}s+\omega_{s1}^2}{s^2+2\xi\varpi_{s1}s+\varpi_{s1}^2}\right) \quad (2\text{-}10)$$

where:

$\omega_{s1} = \sqrt{c_{torsional}/I_1}$

$c_{torsional} = (k_a + k_b)r^2$

θ = azimuth servo angle

I_1 = moment of inertia of the azimuth base structure

B = viscous friction coefficient

ξ = structural damping

ω_{s1} = resonance frequency

ϖ_{s1} = near-to resonance frequency

$\delta\theta$ = incremental angular deflection

k_a, k_b = stiffness coefficients

r = distance of bearing points from the center

3. Methodology

The gimbal analysis in this study is conducted using RecurDyn V9R1 software. It is a computer-aided engineering (CAE) software package whose primary function is the simulation of Multi-Body Dynamics (MBD) for both rigid and flexible bodies by combining traditional rigid MBD with cutting-edge finite element technology for modeling flexible bodies (FunctionBay, 2022). The Analysis type used in this study is Dynamic/Kinematic analysis. This module allows to simulate the multi-body system and also to conduct modal and stability analysis of any kind of multi-body system.

The gimbal geometry model used is a 3D UAV gimbal of 120x120x80 mm and a camera of 100x40x20 mm as shown in Figure 3-1. The gimbal has three arms and three joints representing the 3D rotational movement. This mechanism allows the gimbal to stabilize the platform for the camera to take pictures or record videos during the UAV flight. The geometry is downloaded from the GrabCAD Community website and imported to the RecurDyn software (Karthikeyan, 2020).

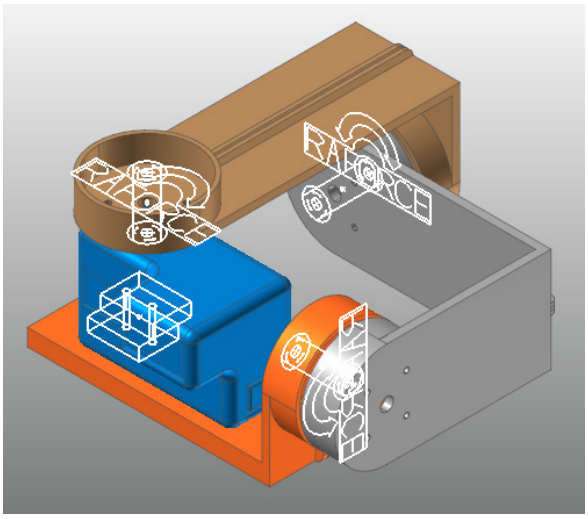

Figure 3-1: Geometry of UAV gimbal and camera used in this study

The arm 1 (brown body) is connected to the ground (UAV body) by a revolute joint. A similar joint also connects the arm 1 with the arm 2 (silver body) and the second arm with the arm 3 (orange body). In each joint, there is a radial force to represent a motor to control the arm rotation. The camera (blue body) is fixed on the arm 3. The material used is steel (default material) and the properties are available in the RecurDyn software as shown in Figure 3-2.

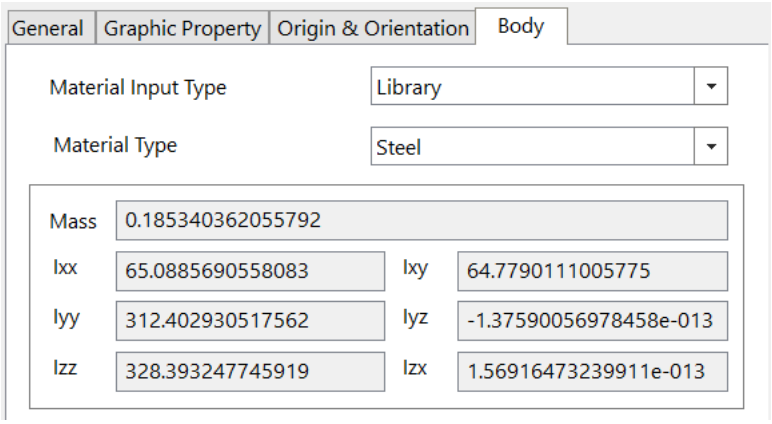

Figure 3-2: Material properties used in this study

Each of the arms is meshed with Solid8 (Hexa8) mesh type, 2 gradation factors, and a relative chordal error ratio of 0.1. The resulting mesh of the gimbal used in this study is shown in Figure 3-3.

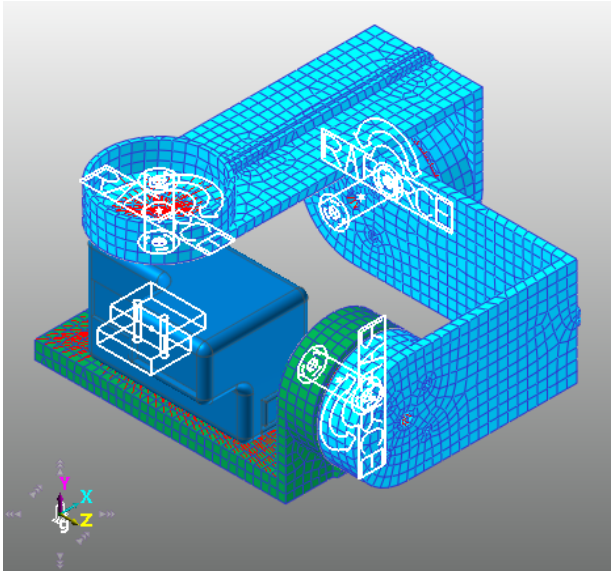

Figure 3-3: Meshed arms of the UAV gimbal

PID controller is used to stabilize the gimbal. The CoLink module in RecurDyn software is used to create the controller. The block diagram of the used PID controller is shown in Figure 3-4. There are two types of output used for this closed-loop feedback which are the rotation angle and the rotation speed of each joint. Each output is connected to the PID controller to become the input of each motor to stabilize the gimbal.

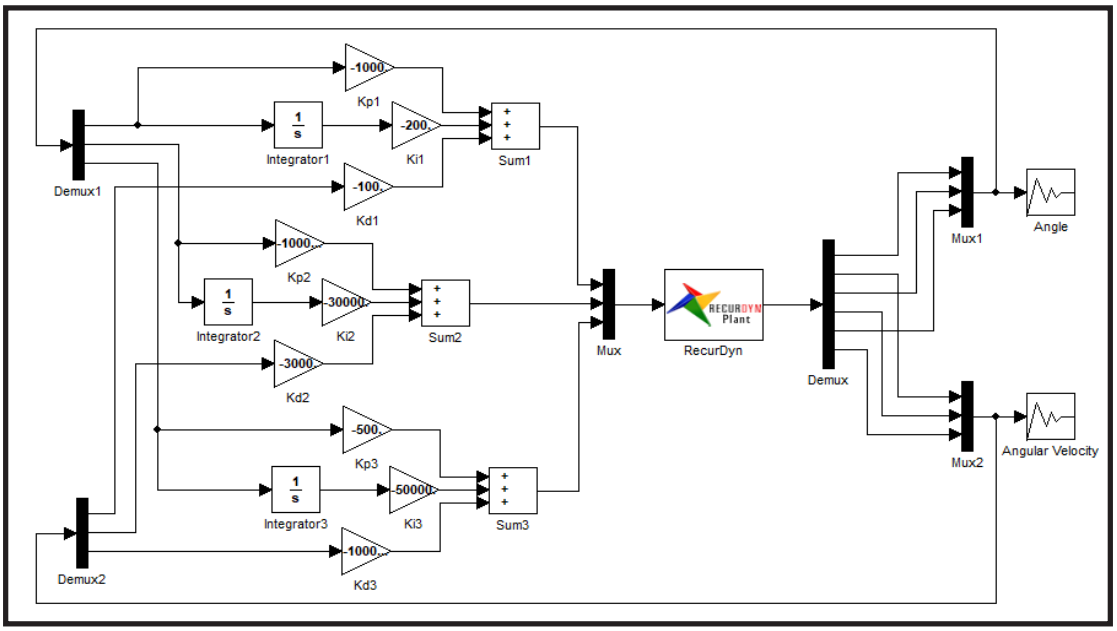

Figure 3-4: PID controller for the gimbal in the CoLink module of RecurDyn

Since the PID gains are very crucial for gimbal stability, at the beginning the gain magnitudes from one of the publications based on Ziegler Nichols and Cohen Coon methods are tried (Rajesh & Ananda, 2015). However, the resulting gimbal movements are not stable. Thus, manual tuning is used to get an acceptable stable result. The tuned gains and resulting gimbal responses are presented in Table 3-1 and Figure 3-5.

In the angular angle response (Figure 3-5 (a)), the angle 1 (yaw angle) is very stable and the angle 2 (roll angle) is asymptotically stable. However, the angle 3 (pitch angle) shows a harmonic response, but very small and hardly visible. It is due to the balancing force at joint 3 that is applied to stabilize the platform that holds a camera. While the effect of the camera weight becomes less on the joint 2 and joint 3 which makes them have more stable responses.

Similarly, the angular velocity response (Figure 3-5 (b)) shows that angular velocity 3 (pitch rate) has a harmonic response but is very small. While the angular velocities 2 and 3 (roll rate and yaw rate) have more stable responses.

Table 3-1: Tuned PID gains for each arm of the gimbal

Arm	Kp	Ki	Kd
Arm 1	-1,000	-200	-100
Arm 2	-100,000	-30,000	-3,000
Arm 3	-500	-50,000	-100,000

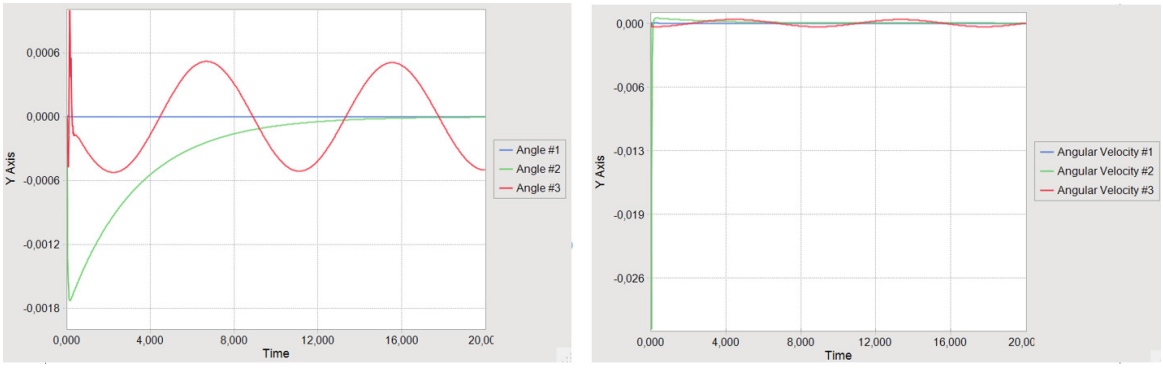

(a) **(b)**

Figure 3-5: Gimbal responds to the tuned PID gains used: (a) Angular angle [rad], (b) Angular velocity [rad/s]

4. Result and Analysis

There are three types of results presented in this section which are disturbance responses, stress analysis, and modal analysis.

4.1. Disturbance Responses

There are 4 types of disturbances considered in this study which are step, pulse, ramp, and sine wave input. It is assumed that the disturbance comes from the UAV. Thus, each disturbance is applied to the revolute joint 1 (yaw angle). The simulation time is selected as 20 s that is considered enough time for the system to respond to the disturbance. The results are shown in Figure 4-1.

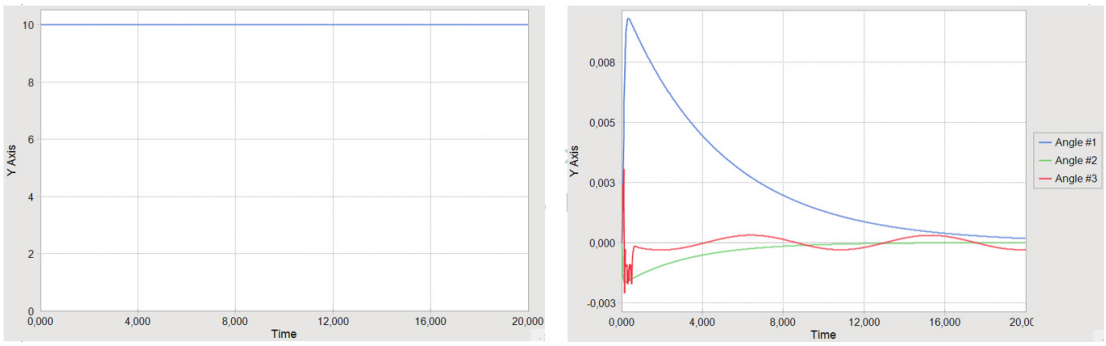

(a) (b)

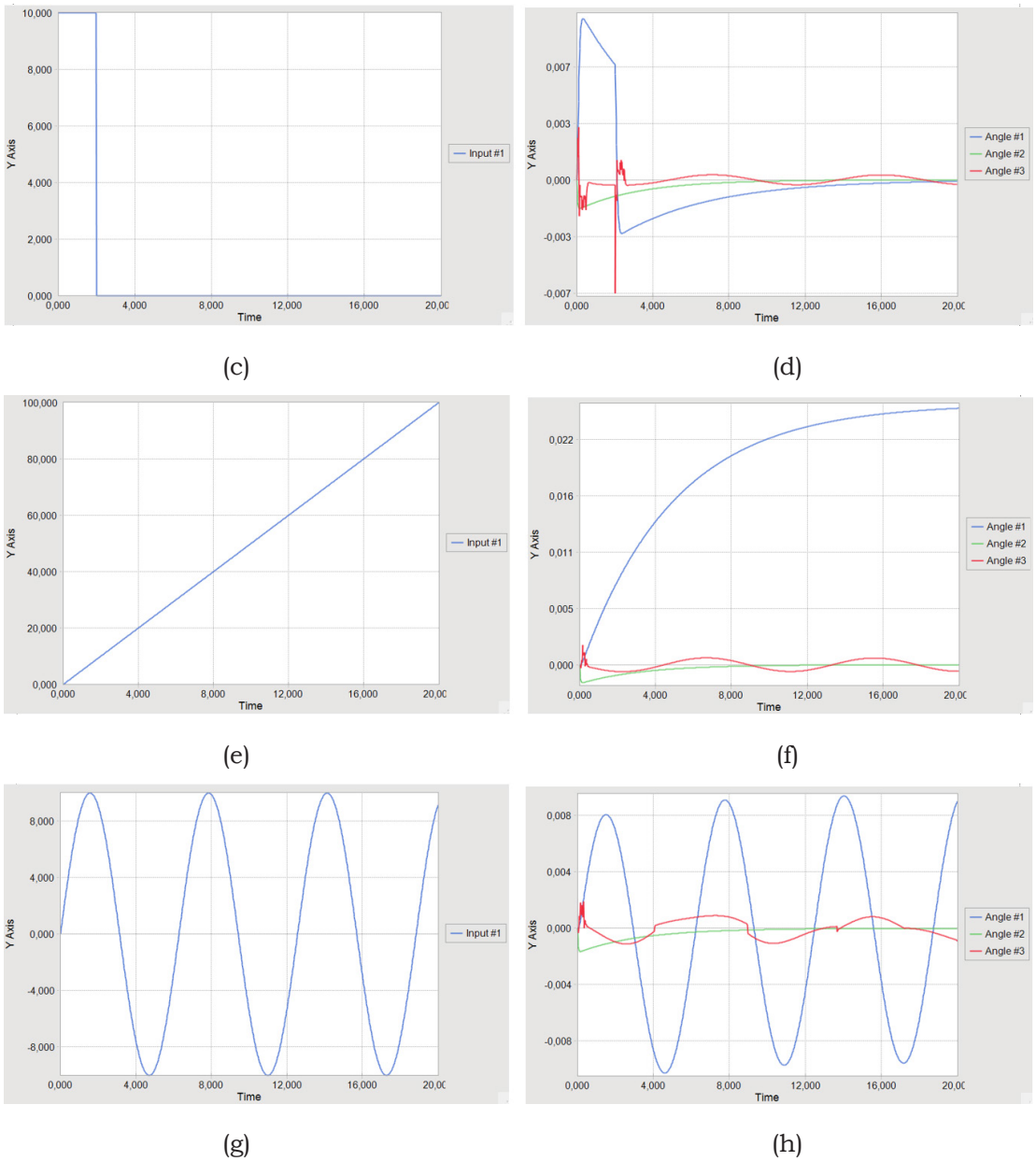

Figure 4-1: Gimbal responds to the disturbances: (a) Step disturbance [N], (b) Angular angle responses to the step disturbance [rad], (c) Pulse disturbance [N], (d) Angular angle responses to the pulse disturbance [rad], (e) Ramp disturbance [N], (f) Angular angle responses to the ramp disturbance [rad], (g) Sine wave disturbance [N], (h) Angular angle responses to the sine wave disturbance [rad],

The angle 1 (yaw angle) responses to the step and pulse disturbances are stable and return asymptotically to zero. While the response to the ramp disturbances is also stable but asymptotically diverts to 0.025 rad. However, the angle 1 response to the sine wave disturbance is not stable and harmonically oscillates following the frequency of the disturbance. It is in line with the finding of another research using PID controller for magnetic levitation systems (Majhi et al., 2015).

The angle 2 (roll angle) responses to all disturbances are stable and asymptotically return to zero. It is the same as the original response at the tuning process of PID gain in Chapter 3. Similarly, the angle 3 (pitch angle) responses to step, impulse, and ramp disturbances are harmonic responses. However, the immediate part of the responses is slightly different due to the type of disturbance. Lastly, the angle 3 response to sine wave disturbance is also a harmonic response but the shape is distorted. Because it is a combination of two disturbances which are from the sine wave and also from the camera weight.

4.2. Stress Analysis

Stress analysis for the gimbal arms is conducted using the FFlex mode in RecurDyn software. The simulation was run for each arm to save the computational speed. The results are shown in Figure 4-2.

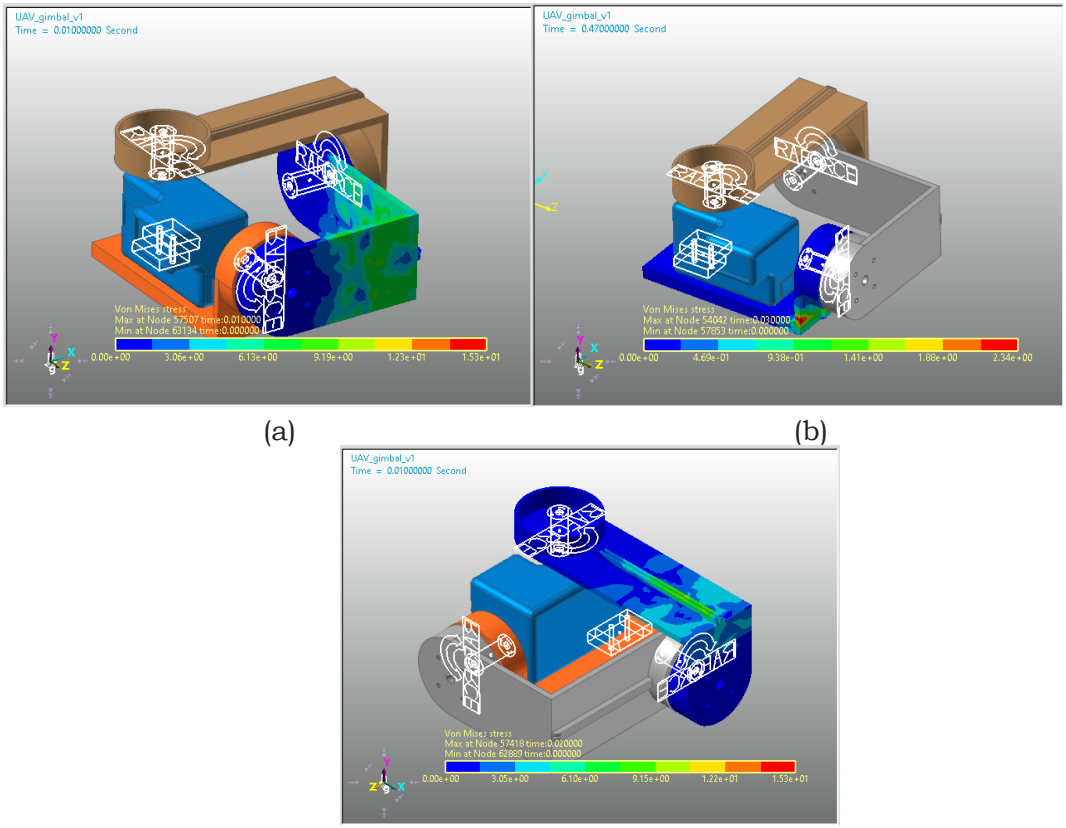

Figure 4-2: Gimbal arms stress analysis: (a) Arm 3, (b) Arm 2, (c) Arm 1

For all results, the most stressful part is the elbow of the arm, but the magnitude and large area are different. The stress at arm 3 concentrated on the small part of the elbow with a maximum stress value of around 2.34 Pa as shown in Figure 4-2 (a). Arm 2 has the largest stress area on both sides of the elbow and the highest stress value of around 9.19 Pa as shown in Figure 4-2 (b). Moreover, arm 1 has a considered large stress area on the elbow with a maximum stress value of around 9.15 Pa as shown in Figure 4-2 (c). This stress phenomenon comes from the effect of gravitation forces from all the components attached to each arm and it is concentrated at the elbow part.

4.3. Modal Analysis

Modal analysis is conducted using the RFlex mode in RecurDyn software. The simulation was run for each arm to save the computational speed. The result of vibration visualization and respective Eigen frequencies are shown in Figure 4-3. The Eigen frequency or natural frequency is the frequency at which a system tends to vibrate in the absence of any external forces.

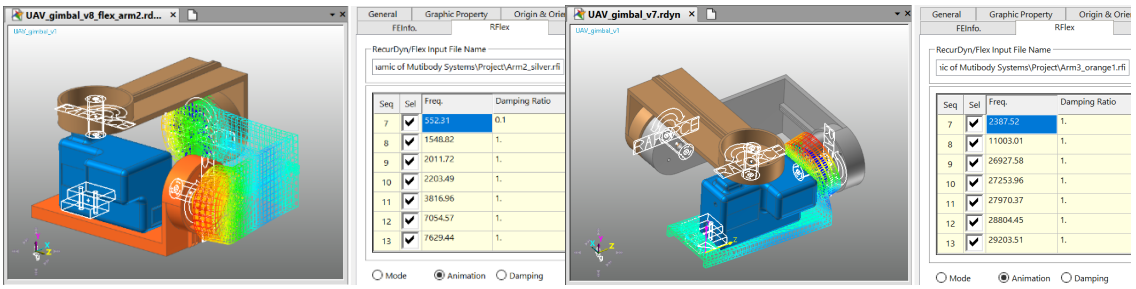

(a) (b)

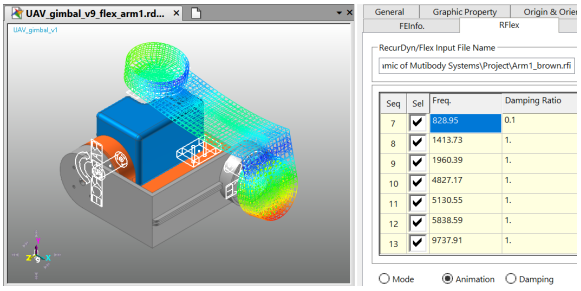

(c)

Figure 4-3: Gimbal arms modal analysis for 7th frequency: (a) Arm 3, (b) Arm 2, (c) Arm 1

For this result, the 7th sequence frequency is analyzed because it is the lowest frequency available. The 1st to 6th sequence result is empty. At the arm 3 (Figure 4-3 (a)), the vibration tends to happen at the connection to the arm 2 with an Eigen frequency of 2,387.52 Hz. While the arm 2 (Figure 4-3 (b)) tends to vibrate at both connectors to arm 1 and arm 3 with an Eigenfrequency of 552.31 Hz. Like the arm 2, the arm 1 (Figure 4-3 (c)) tends to vibrate at both connectors to arm 2 and the ground with an Eigenfrequency of 828.95 Hz. Since the arm 2 has the lowest Eigen frequency, it is more prone to a vibration phenomenon compared to the other arms.

5. Conclusion and Recommendation

This study aims to analyze disturbance effects on UAV gimbal stability and to study stress and modal analysis using flexible body concepts. Based on the result found, the study concludes that:

- 3D gimbal with PID controller needs appropriate gains to be stable.
- PID controller is robust to the impulse, step, and ramp input, but not to the sine wave.
- Structural stress on the gimbal is found on the elbow of the arm.
- The highest value and largest area of stress happen on the arm 2 which connects the arm 1 and arm 3.
- The arm 2 is the most prone to vibration due to the lowest Eigen frequency.

It recommends that these findings could be used by a gimbal manufacturer to strengthen the elbow part of the arms and use a stronger material for the arm 2. Also, other types of materials should be studied to compare the result.

References

Bansal, K., & Dewan, L. (2014). Comparison of Different Controllers for Line- Of-Sight Stabilization of a Gimbal System. *IEEE Students Conference on Engineering and Systems*, 2–6.

Basu, S., Himali, Banerjee, S., & Chaturvedi, S. K. (2019). Modelling and controlling the orientation of an arduino based 3 axis camera gimbal in matlab simulink. *International Journal of Recent Technology and Engineering*, *8*(1), 3049–3053.

FunctionBay. (2022). *RecurDyn Overview*. https://functionbay.com/en/page/single/2/recurdyn-overview

Geng, L., Zhang, Y. F., Wang, P. F., Wang, J. J., Fuh, J. Y. H., & Teo, S. H. (2014). UAV

surveillance mission planning with gimbaled sensors. *IEEE International Conference on Control and Automation, ICCA*, 320–325. https://doi.org/10.1109/ICCA.2014.6870939

Karthikeyan. (2020). *Drone Camera Gimbal*. GrabCAD Community. https://grabcad.com/library/drone-camera-gimbal-1

Krakow, L. W., Eaton, C. M., & Chong, E. K. P. (2018). Simultaneous Non-Myopic Optimization of UAV Guidance and Camera Gimbal Control for Target Tracking. *2018 IEEE Conference on Control Technology and Applications, CCTA 2018*, 349–354. https://doi.org/10.1109/CCTA.2018.8511346

Lin, C. E., & Yang, S. K. (2014). Camera gimbal tracking from UAV flight control. *CACS 2014 - 2014 International Automatic Control Conference, Conference Digest*, *Cacs*, 319–322. https://doi.org/10.1109/CACS.2014.7097209

Majhi, L., Roy, P., & Roy, B. K. (2015). Design of PID and FOPID controllers tuned by firefly algorithm for magnetic levitation system. *Advances in Intelligent Systems and Computing*, *335*(December), 417–430. https://doi.org/10.1007/978-81-322-2217-0_35

Park, J. Y., Kim, S. T., Lee, J. K., Ham, J. W., & Oh, K. Y. (2019). Automatic Inspection Drone with Deep Learning-based Auto-tracking Camera Gimbal to Detect Defects in Power Lines. *ACM International Conference Proceeding Series*. https://doi.org/10.1145/3387168.3387176

Rajesh, R. J., & Ananda, C. M. (2015). PSO tuned PID controller for controlling camera position in UAV using 2-axis gimbal. *Proceedings of the 2015 IEEE International Conference on Power and Advanced Control Engineering, ICPACE 2015*, 128–133. https://doi.org/10.1109/ICPACE.2015.7274930

Rajesh, R. J., & Kavitha, P. (2015). Camera gimbal stabilization using conventional PID controller and evolutionary algorithms. *IEEE International Conference on Computer Communication and Control, IC4 2015*, *September*. https://doi.org/10.1109/IC4.2015.7375580

Sayed, M., Cinca, R., Costanza, E., & Brostow, G. (2022). LookOut! Interactive Camera Gimbal Controller for Filming Long Takes. *ACM Transactions on Graphics*, *41*(3). https://doi.org/10.1145/3506693

Springer, J., & Kyas, M. (2022). Autonomous Precision Drone Landing with Fiducial Markers and a Gimbal-Mounted Camera for Active Tracking. *ArXiv Preprint*, *12*. http://arxiv.org/abs/2206.04617

Sun, M., Zhu, R., & Yang, X. (2008). UAV Path Generation, Path Following and Gimbal Control. *IEEE International Conference on Networking, Sensing and Control*.

Tang, D., Shen, L., & Hu, T. (2019). Online Camera-Gimbal-Odometry System Extrinsic Calibration for Fixed-Wing UAV Swarms. *IEEE Access*, *7*, 146903–146913. https://doi.org/10.1109/ACCESS.2019.2944961

Tiimus, K., & Tamre, M. (2010). Camera gimbal control system for unmanned platforms. *Proceedings of the International Conference of DAAAM Baltic* , *April*.

Wikipedia. (2023). *PID controller*. https://en.wikipedia.org/wiki/PID_controller#Proportional

Zhao, D., Du, Y., Ding, Z., Yuan, B., & Wang, Y. (2022). Experimental Design of Self-Tracking Camera Gimbal Robot Based on OpenCV. *2022 12th International Conference on CYBER Technology in Automation, Control, and Intelligent Systems, CYBER 2022*, 630–635. https://doi.org/10.1109/CYBER55403.2022.9907705